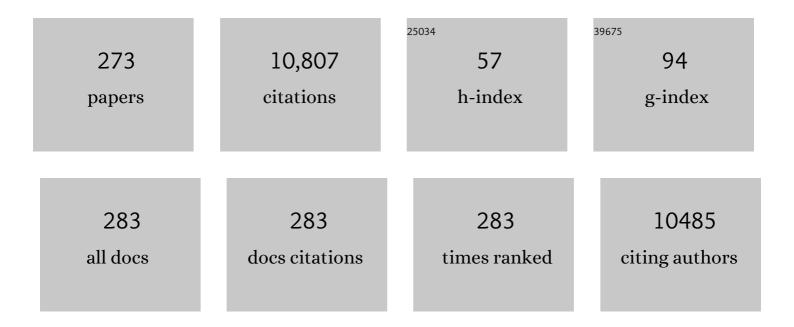
## Tadaaki Nagao

List of Publications by Year in descending order

Source: https://exaly.com/author-pdf/5624238/publications.pdf

Version: 2024-02-01



#	Article	IF	CITATIONS
1	Instability and Charge Density Wave of Metallic Quantum Chains on a Silicon Surface. Physical Review Letters, 1999, 82, 4898-4901.	7.8	543
2	Nanofilm Allotrope and Phase Transformation of Ultrathin Bi Film on Si(111)-7×7. Physical Review Letters, 2004, 93, 105501.	7.8	417
3	Surfaceâ€Plasmonâ€Enhanced Photodriven CO <sub>2</sub> Reduction Catalyzed by Metal–Organicâ€Frameworkâ€Derived Iron Nanoparticles Encapsulated by Ultrathin Carbon Layers. Advanced Materials, 2016, 28, 3703-3710.	21.0	300
4	Role of Spin-Orbit Coupling and Hybridization Effects in the Electronic Structure of Ultrathin Bi Films. Physical Review Letters, 2006, 97, 146803.	7.8	289
5	Titanium Nitride Nanoparticles as Plasmonic Solar Heat Transducers. Journal of Physical Chemistry C, 2016, 120, 2343-2348.	3.1	273
6	Structures and electronic transport on silicon surfaces. Progress in Surface Science, 1999, 60, 89-257.	8.3	210
7	Light-Enhanced Carbon Dioxide Activation and Conversion by Effective Plasmonic Coupling Effect of Pt and Au Nanoparticles. ACS Applied Materials & amp; Interfaces, 2018, 10, 408-416.	8.0	179
8	Electrochemical synthesis of mesoporous gold films toward mesospace-stimulated optical properties. Nature Communications, 2015, 6, 6608.	12.8	178
9	Infrared Perfect Absorbers Fabricated by Colloidal Mask Etching of Al–Al <sub>2</sub> O <sub>3</sub> –Al Trilayers. ACS Photonics, 2015, 2, 964-970.	6.6	172
10	Conversion of Carbon Dioxide by Methane Reforming under Visibleâ€Light Irradiation: Surfaceâ€Plasmonâ€Mediated Nonpolar Molecule Activation. Angewandte Chemie - International Edition, 2015, 54, 11545-11549.	13.8	168
11	Electronic Structures of the Highest Occupied Molecular Orbital Bands of a Pentacene Ultrathin Film. Physical Review Letters, 2007, 98, 247601.	7.8	167
12	Narrowband Wavelength Selective Thermal Emitters by Confined Tamm Plasmon Polaritons. ACS Photonics, 2017, 4, 2212-2219.	6.6	164
13	Direct observation of spin splitting in bismuth surface states. Physical Review B, 2007, 76, .	3.2	163
14	Photo-assisted methanol synthesis via CO2 reduction under ambient pressure over plasmonic Cu/ZnO catalysts. Applied Catalysis B: Environmental, 2019, 250, 10-16.	20.2	142
15	Dispersion and Damping of a Two-Dimensional Plasmon in a Metallic Surface-State Band. Physical Review Letters, 2001, 86, 5747-5750.	7.8	137
16	Design of PdAu alloy plasmonic nanoparticles for improved catalytic performance in CO2 reduction with visible light irradiation. Nano Energy, 2016, 26, 398-404.	16.0	133
17	Infrared Aluminum Metamaterial Perfect Absorbers for Plasmonâ€Enhanced Infrared Spectroscopy. Advanced Functional Materials, 2015, 25, 6637-6643.	14.9	129
18	Examining the Performance of Refractory Conductive Ceramics as Plasmonic Materials: A Theoretical Approach. ACS Photonics, 2016, 3, 43-50.	6.6	126

#	Article	IF	CITATIONS
19	Independently driven four-tip probes for conductivity measurements in ultrahigh vacuum. Surface Science, 2001, 493, 633-643.	1.9	125
20	Effective decoration of Pd nanoparticles on the surface of SnO2 nanowires for enhancement of CO gas-sensing performance. Journal of Hazardous Materials, 2014, 265, 124-132.	12.4	125
21	Light assisted CO 2 reduction with methane over group VIII metals: Universality of metal localized surface plasmon resonance in reactant activation. Applied Catalysis B: Environmental, 2017, 209, 183-189.	20.2	122
22	Ultranarrow-Band Wavelength-Selective Thermal Emission with Aperiodic Multilayered Metamaterials Designed by Bayesian Optimization. ACS Central Science, 2019, 5, 319-326.	11.3	121
23	Si(111)-(×)-Ag surface at low temperatures: symmetry breaking and surface twin boundaries. Surface Science, 1999, 442, 65-73.	1.9	114
24	Na Adsorption on theSi(111)â^'(7×7)Surface: From Two-Dimensional Gas to Nanocluster Array. Physical Review Letters, 2003, 91, 126101.	7.8	110
25	Structural phase transitions ofSi(111)â^'(3×3)R30°â^'Au: Phase transitions in domain-wall configurations. Physical Review B, 1998, 57, 10100-10109.	3.2	106
26	Quantum well states in ultrathin Bi films: Angle-resolved photoemission spectroscopy and first-principles calculations study. Physical Review B, 2007, 75, .	3.2	103
27	One-Dimensional Plasmon in an Atomic-Scale Metal Wire. Physical Review Letters, 2006, 97, 116802.	7.8	101
28	Origin of the Stability of Ge(105) on Si: A New Structure Model and Surface Strain Relaxation. Physical Review Letters, 2002, 88, 176101.	7.8	100
29	Monitoring the Presence of Ionic Mercury in Environmental Water by Plasmon-Enhanced Infrared Spectroscopy. Scientific Reports, 2013, 3, 1175.	3.3	98
30	Hot Electron Excitation from Titanium Nitride Using Visible Light. ACS Photonics, 2016, 3, 1552-1557.	6.6	98
31	Surface electrical conduction due to carrier doping into a surface-state band on Si(111)-3×3-Ag. Physical Review B, 1997, 56, 6782-6787.	3.2	94
32	Longitudinal and transverse coupling in infrared gold nanoantenna arrays: long range versus short range interaction regimes. Optics Express, 2011, 19, 15047.	3.4	94
33	All-Ceramic Microfibrous Solar Steam Generator: TiN Plasmonic Nanoparticle-Loaded Transparent Microfibers. ACS Sustainable Chemistry and Engineering, 2017, 5, 8523-8528.	6.7	93
34	Large surface-state conductivity in ultrathin Bi films. Applied Physics Letters, 2007, 91, .	3.3	92
35	Hole Array Perfect Absorbers for Spectrally Selective Midwavelength Infrared Pyroelectric Detectors. ACS Photonics, 2016, 3, 1271-1278.	6.6	92
36	Moiré Nanosphere Lithography. ACS Nano, 2015, 9, 6031-6040.	14.6	91

#	Article	IF	CITATIONS
37	Thin bismuth film as a template for pentacene growth. Applied Physics Letters, 2005, 86, 073109.	3.3	87
38	Surface-enhanced ATR-IR spectroscopy with interface-grown plasmonic gold-island films near the percolation threshold. Physical Chemistry Chemical Physics, 2011, 13, 4935.	2.8	86
39	Triggering Water and Methanol Activation for Solar-Driven H <sub>2</sub> Production: Interplay of Dual Active Sites over Plasmonic ZnCu Alloy. Journal of the American Chemical Society, 2021, 143, 12145-12153.	13.7	85
40	Plasmonic Janusâ€Composite Photocatalyst Comprising Au and C–TiO <sub>2</sub> for Enhanced Aerobic Oxidation over a Broad Visibleâ€Light Range. Advanced Functional Materials, 2014, 24, 7754-7762.	14.9	83
41	Insulator-to-Proton-Conductor Transition in a Dense Metal–Organic Framework. Journal of the American Chemical Society, 2015, 137, 6428-6431.	13.7	83
42	Origin of flat morphology and high crystallinity of ultrathin bismuth films. Surface Science, 2007, 601, 3593-3600.	1.9	79
43	Spectrally Selective Midâ€Infrared Thermal Emission from Molybdenum Plasmonic Metamaterial Operated up to 1000 °C. Advanced Optical Materials, 2016, 4, 1987-1992.	7.3	79
44	Structural phase transitions of Pb-adsorbed Si(111) surfaces at low temperatures. Physical Review B, 1999, 60, 13287-13290.	3.2	76
45	Electronic Structure of Ultrathin Bismuth Films with A7 and Black-Phosphorus-like Structures. Journal of the Physical Society of Japan, 2008, 77, 014701.	1.6	73
46	Light assisted CO <sub>2</sub> reduction with methane over SiO <sub>2</sub> encapsulated Ni nanocatalysts for boosted activity and stability. Journal of Materials Chemistry A, 2017, 5, 10567-10573.	10.3	71
47	Solar water heating and vaporization with silicon nanoparticles at mie resonances. Optical Materials Express, 2016, 6, 640.	3.0	69
48	Color-Tunable Resonant Photoluminescence and Cavity-Mediated Multistep Energy Transfer Cascade. ACS Nano, 2016, 10, 7058-7063.	14.6	67
49	All eramic Solarâ€Driven Water Purifier Based on Anodized Aluminum Oxide and Plasmonic Titanium Nitride. Advanced Sustainable Systems, 2019, 3, 1800112.	5.3	67
50	Strong lateral growth and crystallization via two-dimensional allotropic transformation of semi-metal Bi film. Surface Science, 2005, 590, 247-252.	1.9	66
51	Enhanced Solar Light Absorption and Photoelectrochemical Conversion Using TiN Nanoparticle-Incorporated C <sub>3</sub> N <sub>4</sub> –C Dot Sheets. ACS Applied Materials & Interfaces, 2018, 10, 2460-2468.	8.0	64
52	Metamaterial-enhanced vibrational absorption spectroscopy for the detection of protein molecules. Scientific Reports, 2016, 6, 32123.	3.3	63
53	Origin of the surface-state band-splitting in ultrathin Bi films: from a Rashba effect to a parity effect. New Journal of Physics, 2008, 10, 083038.	2.9	62
54	Antenna Sensing of Surface Phonon Polaritons. Journal of Physical Chemistry C, 2010, 114, 7299-7301.	3.1	62

#	Article	IF	CITATIONS
55	Radiative cooling for continuous thermoelectric power generation in day and night. Applied Physics Letters, 2020, 117, .	3.3	62
56	Fabrication of Highly Metallic TiN Films by Pulsed Laser Deposition Method for Plasmonic Applications. ACS Photonics, 2018, 5, 814-819.	6.6	60
57	Hybridizing Poly(ε-caprolactone) and Plasmonic Titanium Nitride Nanoparticles for Broadband Photoresponsive Shape Memory Films. ACS Applied Materials & Interfaces, 2016, 8, 5634-5640.	8.0	59
58	A series of Ca-induced reconstructions on Si(111) surface. Surface Science, 2001, 493, 148-156.	1.9	58
59	Tamm plasmon selective thermal emitters. Optics Letters, 2016, 41, 4453.	3.3	58
60	Nonmetallic Materials for Plasmonic Hot Carrier Excitation. Advanced Optical Materials, 2019, 7, 1800603.	7.3	58
61	Electron standing waves on the Si(111)-3×3-Ag surface. Physical Review B, 1999, 59, 2035-2039.	3.2	57
62	Surface-State Bands on Silicon –Si(111)-\$sqrt{3}imessqrt{3}\$-Ag Surface Superstructure–. Japanese Journal of Applied Physics, 2000, 39, 3815-3822.	1.5	55
63	Growth and electron quantization of metastable silver films on Si(001). Physical Review B, 2001, 63, .	3.2	54
64	Chemically synthesized nanowire TiO2/ZnO core-shell p-n junction array for high sensitivity ultraviolet photodetector. Applied Physics Letters, 2013, 103, .	3.3	52
65	Morphology of ultrathin manganese silicide on Si(111). Surface Science, 1999, 419, 134-143.	1.9	51
66	Two-dimensional adatom gas phase on the Si(111)-3×3-Ag surface directly observed by scanning tunneling microscopy. Physical Review B, 1999, 60, 16083-16087.	3.2	49
67	Phase transition and stability of Si(111)–8×`2'-In surface phase at low temperatures. Surface Science, 2001, 488, 15-22.	1.9	49
68	Electronic structure of Ag-induced3×3and21×21superstructures on the Si(111) surface studied by angle-resolved photoemission spectroscopy and scanning tunneling microscopy. Physical Review B, 2001, 64, .	3.2	49
69	STM observations of Ag adsorption on the Si(111)– surface at low temperatures. Surface Science, 1998, 408, 146-159.	1.9	48
70	Porous gold nanodisks with multiple internal hot spots. Physical Chemistry Chemical Physics, 2012, 14, 9131.	2.8	48
71	Surface pre-melting and surface flattening of Bi nanofilms on Si(111)-7×7. Surface Science, 2003, 547, L877-L881.	1.9	47
72	In situ Surface-Enhanced Infrared Absorption Spectroscopy for the Analysis of the Adsorption and Desorption Process of Au Nanoparticles on the SiO2/Si Surface. Langmuir, 2007, 23, 6119-6125.	3.5	47

#	Article	IF	CITATIONS
73	Microstructure of leached Al-Cu-Fe quasicrystal with high catalytic performance for steam reforming of methanol. Applied Catalysis A: General, 2010, 384, 241-251.	4.3	47
74	Plasmons in nanoscale and atomic-scale systems. Science and Technology of Advanced Materials, 2010, 11, 054506.	6.1	47
75	Epitaxial Growth of Single-Crystal Ultrathin Films of Bismuth on Si(111). Japanese Journal of Applied Physics, 2000, 39, 4567-4570.	1.5	46
76	Conjugated Polymer Blend Microspheres for Efficient, Long-Range Light Energy Transfer. ACS Nano, 2016, 10, 5543-5549.	14.6	46
77	Whispering Gallery Resonance from Self-Assembled Microspheres of Highly Fluorescent Isolated Conjugated Polymers. Macromolecules, 2015, 48, 3928-3933.	4.8	45
78	Electrical conduction via surface-state bands. Surface Science, 1997, 386, 322-327.	1.9	44
79	A synergistic interaction between isolated Au nanoparticles and oxygen vacancies in an amorphous black TiO <sub>2</sub> nanoporous film: toward enhanced photoelectrochemical water splitting. Journal of Materials Chemistry A, 2018, 6, 12978-12984.	10.3	44
80	High quality thermochromic VO2 films prepared by magnetron sputtering using V2O5 target with in situ annealing. Applied Surface Science, 2019, 495, 143436.	6.1	44
81	Angstrom-Scale Distance Dependence of Antenna-Enhanced Vibrational Signals. ACS Nano, 2012, 6, 10917-10923.	14.6	43
82	Structure ofC60layers on theSi(111)â^'3×3â^'Agsurface. Physical Review B, 1999, 60, 11131-11136.	3.2	39
83	Reversible adsorption of Au nanoparticles on SiO2/Si: An in situ ATR-IR study. Surface Science, 2006, 600, L71-L75.	1.9	39
84	Strong coupling between phonon-polaritons and plasmonic nanorods. Optics Express, 2016, 24, 25528.	3.4	39
85	Experimental investigation of two-dimensional plasmons in a <mml:math xmlns:mml="http://www.w3.org/1998/Math/MathML" display="inline"&gt;<mml:mrow><mml:msub><mml:mrow><mml:mtext>DySi</mml:mtext></mml:mrow><mml:mr on Si(111), Physical Review B, 2008, 78, .</mml:mr </mml:msub></mml:mrow></mml:math 	ı>2 <sup>3;2</sup> mml:	mn <sup>38</sup>
86	Band engineering of ternary metal nitride system Ti_1-x Zr_xN for plasmonic applications. Optical Materials Express, 2016, 6, 29.	3.0	37
87	Tunable Nanoantennas for Surface Enhanced Infrared Absorption Spectroscopy by Colloidal Lithography and Post-Fabrication Etching. Scientific Reports, 2017, 7, 44069.	3.3	37
88	Stability of the quasicubic phase in the initial stage of the growth of bismuth films on Si(111)-7×7. Journal of Applied Physics, 2006, 99, 014904.	2.5	36
89	Optical microresonator arrays of fluorescence-switchable diarylethenes with unreplicable spectral fingerprints. Materials Horizons, 2020, 7, 1801-1808.	12.2	36
90	Dual roles of a transparent polymer film containing dispersed N-doped carbon dots: A high-efficiency blue light converter and UV screen. Applied Surface Science, 2020, 510, 145405.	6.1	36

#	Article	IF	CITATIONS
91	Two-dimensional adatom gas on the Si(111)-(â^š3×â^š3)-Ag surface detected through changes in electrical conduction. Physical Review B, 1996, 54, 14134-14138.	3.2	35
92	MICRO-FOUR-POINT PROBES IN A UHV SCANNING ELECTRON MICROSCOPE FOR IN-SITU SURFACE-CONDUCTIVITY MEASUREMENTS. Surface Review and Letters, 2000, 07, 533-537.	1.1	34
93	Terahertz-Field-Induced Nonlinear Electron Delocalization in Au Nanostructures. Nano Letters, 2015, 15, 1036-1040.	9.1	34
94	Effect of different surfactants on structural and optical properties of Ce3+ and Tb3+ co-doped BiPO4 nanostructures. Optical Materials, 2015, 39, 110-117.	3.6	34
95	Resonant Optical Absorption and Photothermal Process in High Refractive Index Germanium Nanoparticles. Advanced Optical Materials, 2017, 5, 1600902.	7.3	34
96	Narrowâ€Band Thermal Emitter with Titanium Nitride Thin Film Demonstrating High Temperature Stability. Advanced Optical Materials, 2020, 8, 1900982.	7.3	34
97	Oxygen adsorption sites on the PrB6(100) and LaB6(100) surfaces. Surface Science, 1996, 348, 133-142.	1.9	33
98	Visible-light photodecomposition of acetaldehyde by TiO <sub>2</sub> -coated gold nanocages: plasmon-mediated hot electron transport via defect states. Chemical Communications, 2014, 50, 15553-15556.	4.1	33
99	Broadband Plasmon Resonance Enhanced Third-Order Optical Nonlinearity in Refractory Titanium Nitride Nanostructures. ACS Photonics, 2018, 5, 3452-3458.	6.6	33
100	Photocurrent Enhancements of TiO <sub>2</sub> -Based Nanocomposites with Gold Nanostructures/Reduced Graphene Oxide on Nanobranched Substrate. Journal of Physical Chemistry C, 2019, 123, 21103-21113.	3.1	33
101	One-dimensional plasmons in ultrathin metallic silicide wires of finite width. Physical Review B, 2010, 81, .	3.2	32
102	An On hip Quadâ€Wavelength Pyroelectric Sensor for Spectroscopic Infrared Sensing. Advanced Science, 2019, 6, 1900579.	11.2	31
103	Surface metallic states in ultrathin Bi(001) films studied with terahertz time-domain spectroscopy. Applied Physics Letters, 2012, 100, 251605.	3.3	30
104	Structure and optical properties of sputter deposited pseudobrookite Fe <sub>2</sub> TiO <sub>5</sub> thin films. CrystEngComm, 2019, 21, 34-40.	2.6	30
105	Plasmon-mediated photocatalytic activity of wet-chemically prepared ZnO nanowire arrays. Physical Chemistry Chemical Physics, 2015, 17, 7395-7403.	2.8	29
106	Tunable multiband metasurfaces by moir $ ilde{A}$ © nanosphere lithography. Nanoscale, 2015, 7, 20391-20396.	5.6	29
107	Sub-Band Gap Photodetection from the Titanium Nitride/Germanium Heterostructure. ACS Applied Materials & amp; Interfaces, 2019, 11, 21965-21972.	8.0	28
108	Carbon Dot/Cellulose-Based Transparent Films for Efficient UV and High-Energy Blue Light Screening. ACS Sustainable Chemistry and Engineering, 2021, 9, 9879-9890.	6.7	28

#	Article	IF	CITATIONS
109	Role of Oxygen Electrons in the Metal-Insulator Transition in the Magnetoresistive Oxide <mml:math xmlns:mml="http://www.w3.org/1998/Math/MathML" display="inline"&gt;<mml:msub><mml:mi>La</mml:mi><mml:mrow><mml:mn>2</mml:mn><mml:mo>â^`</mml:mo> mathvari. Physical Review Letters, 2009, 102, 206402.</mml:mrow></mml:msub></mml:math 	> <b>7.8</b> ≻≺mml:mr	.≯ <b>2</b>
110	Infrared spectroscopic and electron microscopic characterization of gold nanogap structure fabricated by focused ion beam. Nanotechnology, 2011, 22, 275202.	2.6	27
111	Active molecular plasmonics: tuning surface plasmon resonances by exploiting molecular dimensions. Nanophotonics, 2015, 4, 186-197.	6.0	26
112	Plasmonic–Photonic Hybrid Modes Excited on a Titanium Nitride Nanoparticle Array in the Visible Region. ACS Photonics, 2017, 4, 815-822.	6.6	26
113	FRET-mediated near infrared whispering gallery modes: studies on the relevance of intracavity energy transfer with <i>Q</i> -factors. Materials Chemistry Frontiers, 2018, 2, 270-274.	5.9	26
114	Disappearance of the quasi-one-dimensional plasmon at the metal-insulator phase transition of indium atomic wires. Physical Review B, 2008, 77, .	3.2	24
115	Demonstration of temperature-plateau superheated liquid by photothermal conversion of plasmonic titanium nitride nanostructures. Nanoscale, 2018, 10, 18451-18456.	5.6	24
116	Marimo-Bead-Supported Core–Shell Nanocomposites of Titanium Nitride and Chromium-Doped Titanium Dioxide as a Highly Efficient Water-Floatable Green Photocatalyst. ACS Applied Materials & Interfaces, 2020, 12, 31327-31339.	8.0	24
117	Vibrations of alkali-metal atoms chemisorbed on the Al(111) surface. Surface Science, 1995, 329, 269-275.	1.9	23
118	Critical scattering at the order-disorder phase transition of Si(111)-3×3R30°-Au surface: A phase transition with particle exchange. Physical Review B, 1997, 55, 8129-8135.	3.2	23
119	Two-dimensional plasmon in a metallic monolayer on a semiconductor surface: Exchange-correlation effects. Physical Review B, 2002, 66, .	3.2	23
120	Sound-Wave-Like Collective Electronic Excitations in Au Atom Chains. Journal of the Physical Society of Japan, 2007, 76, 114714.	1.6	23
121	Optical detection of plasmonic and interband excitations in 1-nm-wide indium atomic wires. Applied Physics Letters, 2010, 96, 243101.	3.3	23
122	Proteinâ€Functionalized Indiumâ€Tin Oxide Nanoantenna Arrays for Selective Infrared Biosensing. Advanced Optical Materials, 2017, 5, 1700091.	7.3	23
123	Dual-band <i>in situ</i> molecular spectroscopy using single-sized Al-disk perfect absorbers. Nanoscale, 2019, 11, 9508-9517.	5.6	22
124	Selective patterned growth of ZnO nanowires/nanosheets and their photoluminescence properties. Optical Materials Express, 2015, 5, 353.	3.0	21
125	Anti-reflection textured structures by wet etching and island lithography for surface-enhanced Raman spectroscopy. Applied Surface Science, 2015, 357, 615-621.	6.1	20
126	Light-promoted conversion of greenhouse gases over plasmonic metal–carbide nanocomposite catalysts. Materials Chemistry Frontiers, 2018, 2, 580-584.	5.9	20

ΤΑDΑΑΚΙ ΝΑGΑΟ

#	:	Article	IF	CITATIONS
1	27	Selective thermal emitters with infrared plasmonic indium tin oxide working in the atmosphere. Optical Materials Express, 2019, 9, 2534.	3.0	20
1	28	Two-dimensional plasmon in a surface-state band. Surface Science, 2001, 493, 680-686.	1.9	19
1	29	Ultrafast phonon dynamics of epitaxial atomic layers of Bi on Si(111). Physical Review B, 2015, 91, .	3.2	19
1	30	MEMS-Based Wavelength-Selective Bolometers. Micromachines, 2019, 10, 416.	2.9	19
1	31	Device Architecture for Visible and Near-Infrared Photodetectors Based on Two-Dimensional SnSe2 and MoS2: A Review. Micromachines, 2020, 11, 750.	2.9	19
1	32	Surface phonons of Na-induced superstructures on Al(111). Physical Review B, 1997, 55, 10064-10073.	3.2	18
1	33	Magnetically Assembled Ni@Ag Urchinâ€Like Ensembles with Ultraâ€Sharp Tips and Numerous Gaps for SERS Applications. Small, 2014, 10, 2564-2569.	10.0	18
1	34	Midâ€infrared optical and electrical properties of indium tin oxide films. Physica Status Solidi (A) Applications and Materials Science, 2017, 214, 1600467.	1.8	18
1	35	Extreme thermal anisotropy in high-aspect-ratio titanium nitride nanostructures for efficient photothermal heating. Nanophotonics, 2021, 10, 1487-1494.	6.0	18
1	36	Deformation of octahedra at LaB6(100) surface studied by HREELS. Surface Science, 1993, 287-288, 391-395.	1.9	17
1	37	Oxygen adsorption on LaB6 (100) and (111) surfaces. Surface Science, 1996, 357-358, 708-711.	1.9	17
1	38	Plasmon-mediated photothermal conversion by TiN nanocubes toward CO oxidation under solar light illumination. RSC Advances, 2016, 6, 110566-110570.	3.6	17
1	39	Construction of a highâ€resolution electron energy loss spectrometer. Review of Scientific Instruments, 1994, 65, 515-516.	1.3	16
14	40	Surface electronic transport on silicon: donor- and acceptor-type adsorbates on Si(111)-â^š3×â^š3-Ag substrate. Applied Surface Science, 2000, 162-163, 42-47.	6.1	16
1	41	Step-by-step cooling of a two-dimensional Na gas on theSi(111)â€(7×7)surface. Physical Review B, 2004, 70, .	3.2	16
1	42	A MEMS-Based Quad-Wavelength Hybrid Plasmonic–Pyroelectric Infrared Detector. Micromachines, 2019, 10, 413.	2.9	16
1	43	Effects of Ag particle geometry on photocatalytic performance of Ag/TiO2/reduced graphene oxide ternary systems. Materials Chemistry and Physics, 2020, 240, 122216.	4.0	16
		Tereberts Fereday and Kerr retation an estragoon of umplimeth		

Terahertz Faraday and Kerr rotation spectroscopy of <mml:math xmlns:mml="http://www.w3.org/1998/Math/MathML"><mml:mrow><mml:msub><mml:mi>Bi</mml:mi><mml:mrow2<mml:mba>1</mml films in high magnetic fields up to 30 tesla. Physical Review B, 2019, 100, .

#	Article	IF	CITATIONS
145	Hydropower generation by transpiration from microporous alumina. Scientific Reports, 2021, 11, 10954.	3.3	15
146	Excitation Induced Tunable Emission in Ce <sup><b>3+</b></sup> /Eu <sup><b>3+</b></sup> Codoped BiPO <sub><b>4</b></sub> Nanophosphors. Journal of Spectroscopy, 2015, 2015, 1-10.	1.3	14
147	Synthesis, structural, and electrical characterization of RuO2 sol–gel spin-coating nano-films. Journal of Materials Science: Materials in Electronics, 2016, 27, 10791-10797.	2.2	14
148	Design of a silicon-based plasmonic optical sensor for magnetic field monitoring in the infrared. Applied Physics B: Lasers and Optics, 2014, 117, 363-368.	2.2	13
149	Terahertz-induced acceleration of massive Dirac electrons in semimetal bismuth. Scientific Reports, 2015, 5, 15870.	3.3	13
150	Self-assembled polycarbazole microspheres as single-component, white-colour resonant photoemitters. RSC Advances, 2016, 6, 52854-52857.	3.6	13
151	Effect of oxygen annealing on the photoresponse of PbSe thin films fabricated by the pulsed laser deposition method. Radiation Effects and Defects in Solids, 2018, 173, 112-117.	1.2	13
152	Laser-induced structural disordering and optical phase change in semimetal bismuth observed by Raman microscopy. Applied Surface Science, 2019, 491, 675-681.	6.1	13
153	Transparent Hard Coatings with SiON-Encapsulated N-Doped Carbon Dots for Complete UV Blocking and White Light Emission. ACS Applied Electronic Materials, 2021, 3, 3761-3773.	4.3	13
154	Deformation of boron networks at the LaB6(111) surface. Surface Science, 1998, 416, 363-370.	1.9	12
155	Surface Electrical Conduction Correlated with Surface Structures and Atom Dynamics. Surface Review and Letters, 1998, 05, 803-819.	1.1	12
156	Growth mode and electrical conductance of Ag atomic layers on Si( 001 ) surface. Surface Science, 2001, 493, 389-398.	1.9	12
157	Fluorine etching on the Si()-7×7 surfaces using fluorinated fullerene. Surface Science, 2002, 521, 43-48.	1.9	12
158	Exchange-Correlation Effects on Low-Dimensional Plasmons in an Array of Metallic Quantum Wires. Materials Transactions, 2007, 48, 718-721.	1.2	12
159	Wavelength-selective spin-current generator using infrared plasmonic metamaterials. APL Photonics, 2017, 2, .	5.7	12
160	Quantifying photoinduced carriers transport in exciton–polariton coupling of MoS2 monolayers. Npj 2D Materials and Applications, 2021, 5, .	7.9	12
161	Diffraction from small antiphase domains: α-, β-, 6×6 phases of Au adsorbed Si(111). Applied Surface Science, 1998, 130-132, 47-53.	6.1	11
162	Construction of an ELS-LEED: an electron energy-loss spectrometer with electrostatic two-dimensional angular scanning. Surface and Interface Analysis, 2000, 30, 488-492.	1.8	11

#	Article	IF	CITATIONS
163	Comparative Study of Atomic and Electronic Structures of P and Bi Nanofilms. Japanese Journal of Applied Physics, 2007, 46, 7824-7828.	1.5	11
164	White Light Emission from Black Germanium. ACS Photonics, 2017, 4, 1722-1729.	6.6	11
165	Optically monitored wetâ€chemical preparation of SEIRA active Au nanostructures. Surface and Interface Analysis, 2008, 40, 1681-1683.	1.8	10
166	The excitation of one-dimensional plasmons in Si and Au–Si complex atom wires. Nanotechnology, 2008, 19, 355204.	2.6	10
167	Low-energy plasmons in quantum-well and surface states of metallic thin films. Physical Review B, 2011, 84, .	3.2	10
168	Carbon nanotube mat as substrate for ZnO nanotip field emitters. RSC Advances, 2012, 2, 2713.	3.6	10
169	Far-field and near-field monitoring of hybridized optical modes from Au nanoprisms suspended on a graphene/Si nanopillar array. Nanoscale, 2017, 9, 16950-16959.	5.6	10
170	Thermochromic vanadium dioxide film on textured silica substrate for smart window with enhanced visible transmittance and tunable infrared radiation. Infrared Physics and Technology, 2019, 102, 103019.	2.9	10
171	Direct Observation of Photoinduced Charge Separation at Transition-Metal Nitride–Semiconductor Interfaces. ACS Applied Materials & Interfaces, 2020, 12, 56562-56567.	8.0	10
172	Effects of nanoscale morphology and defects in oxide: optoelectronic functions of zinc oxide nanowires. Radiation Effects and Defects in Solids, 2016, 171, 22-33.	1.2	9
173	Enhanced photocurrent generation from indium–tin-oxide/Fe2TiO5 hybrid nanocone arrays. Nano Energy, 2020, 76, 104965.	16.0	9
174	Simultaneous harvesting of radiative cooling and solar heating for transverse thermoelectric generation. Science and Technology of Advanced Materials, 2021, 22, 441-448.	6.1	9
175	Surface Phonon Dispersion Curves of NiAl(111). Japanese Journal of Applied Physics, 1993, 32, 3252-3256.	1.5	8
176	Surface phonon dispersion curves of the LaB6(111) surface. Surface Science, 1996, 357-358, 712-716.	1.9	8
177	Vibrational spectra of oxygen on LaB6(100), (110), and (111) surfaces: A comparative study using high resolution electron energy loss spectroscopy. Journal of Vacuum Science and Technology A: Vacuum, Surfaces and Films, 1996, 14, 1674-1678.	2.1	8
178	Surface roughness and electrical resistance on Si( 100 )2×3-Na surface. Surface Science, 2001, 493, 619-625.	1.9	8
179	Precisely Controlled Fabrication of a Highly Sensitive Au Sensor Film for Surface Enhanced Spectroscopy. Japanese Journal of Applied Physics, 2007, 46, L1222-L1224.	1.5	8
180	Arrays of Nanoscale Gold Dishes Containing Engineered Substructures. Advanced Optical Materials, 2013, 1, 814-818.	7.3	8

#	Article	IF	CITATIONS
181	Fabrication of plasmonic nanopillar arrays based on nanoforming. Microelectronic Engineering, 2015, 139, 7-12.	2.4	8
182	Transparent oxides forming conductor/insulator/conductor heterojunctions for photodetection. Nanotechnology, 2015, 26, 215203.	2.6	8
183	Improvement of smooth surface of RuO2 bottom electrode on Al2O3 buffer layer and characteristics of RuO2/TiO2/Al2O3/TiO2/RuO2 capacitors. Journal of Vacuum Science and Technology A: Vacuum, Surfaces and Films, 2017, 35, .	2.1	8
184	Dark-Field Scattering and Local SERS Mapping from Plasmonic Aluminum Bowtie Antenna Array. Micromachines, 2019, 10, 468.	2.9	8
185	Graphene-Loaded Plasmonic Zirconium Nitride and Gold Nanogroove Arrays for Surface-Charge Modifications. ACS Applied Nano Materials, 2020, 3, 5002-5007.	5.0	8
186	Gires-Tournois resonators as ultra-narrowband perfect absorbers for infrared spectroscopic devices. Optics Express, 2019, 27, A725.	3.4	8
187	Diffusion anisotropy of Ag and In on Si(111) surface studied by UHV-SEM. Ultramicroscopy, 2000, 85, 23-33.	1.9	7
188	Nonlinear mechanism of plasmon damping in electron gas. Physical Review B, 2002, 66, .	3.2	7
189	Layer-by-layer growth of Ag on a GaN(0001) surface. Applied Physics Letters, 2003, 82, 1389-1391.	3.3	7
190	Bilayer-by-bilayer etching of 6H-GaN(0001) with Cl. Surface Science, 2004, 561, L213-L217.	1.9	7
191	Softening versus hardening transition in surface bilayer bonding of bismuth nanofilm. Physical Review B, 2010, 82, .	3.2	7
192	Thickness dependent phase transition of Bi films quench condensed on semiconducting surfaces. CrystEngComm, 2011, 13, 4604.	2.6	7
193	Optical Properties of Au-Based and Pt-Based Alloys for Infrared Device Applications: A Combined First Principle and Electromagnetic Simulation Study. Micromachines, 2019, 10, 73.	2.9	7
194	Ultrafast optical modulation of Dirac electrons in gated single-layer graphene. Physical Review B, 2020, 101, .	3.2	7
195	Edge States of Bi Nanoribbons on Bi Substrates: First-Principles Density Functional Study. Japanese Journal of Applied Physics, 2012, 51, 025201.	1.5	7
196	Two-Step Desorption Process of Au Nanoparticles in D2O Suspension on Amino-Terminated SiO2/Si Substrate Induced by Small Thiol Molecules. Japanese Journal of Applied Physics, 2007, 46, 3020-3023.	1.5	6
197	Fluorine diffusion assisted by diffusing silicon on the Si(111)-(7×7) surface. Journal of Chemical Physics, 2008, 129, 234710.	3.0	6
198	Edge States of Bi Nanoribbons on Bi Substrates: First-Principles Density Functional Study. Japanese Journal of Applied Physics, 2012, 51, 025201.	1.5	6

#	Article	IF	CITATIONS
199	Optical properties of ordered Dot-on-Plate nano-sandwich arrays. Microelectronic Engineering, 2014, 127, 34-39.	2.4	6
200	Plasmon mediated cathodic photocurrent generation in sol-gel synthesized doped SrTiO3 nanofilms. APL Materials, 2015, 3, .	5.1	6
201	Solar-active titanium-based oxide photocatalysts loaded on TiN array absorbers for enhanced broadband photocurrent generation. Journal of Applied Physics, 2021, 129, .	2.5	6
202	Direct imaging of visible-light-induced one-step charge separation at the chromium( <scp>iii</scp> ) oxide–strontium titanate interface. Journal of Materials Chemistry A, 2022, 10, 752-761.	10.3	6
203	Hydrogen-Induced Instability of the Ge(105) Surface. Physical Review Letters, 2005, 94, 086105.	7.8	5
204	Characterization of atomicâ€level plasmonic structures by lowâ€energy EELS. Surface and Interface Analysis, 2008, 40, 1764-1767.	1.8	5
205	Studies on gold atom chains and lead nanowires on silicon vicinal surfaces. Journal of Physics: Conference Series, 2009, 187, 012025.	0.4	5
206	Thermodynamically stable nanotips of Au–Mo alloy. Journal of Vacuum Science & Technology B, 2009, 27, 2432-2434.	1.3	5
207	Characteristic IR Câ•C Stretch Enhancement in Monolayers by Nonconjugated, Noncumulated Unsaturated Bonds. Langmuir, 2010, 26, 4594-4597.	3.5	5
208	Plasmonic mesostructures with aligned hotspots on highly oriented mesoporous silica films. Optical Materials Express, 2016, 6, 2824.	3.0	5
209	Nanoantenna Structure with Mid-Infrared Plasmonic Niobium-Doped Titanium Oxide. Micromachines, 2020, 11, 23.	2.9	5
210	Surface atomic structure and surface force constants: Cu(100)2â^š2 × â^š2-R45°-O and LaB6(100). Surface Science, 1993, 298, 450-455.	1.9	4
211	Substrate-Structure Dependence of Ag Electromigration on Au-Precovered Si(111) Surfaces. Japanese Journal of Applied Physics, 2000, 39, 4438-4442.	1.5	4
212	Electromigration and phase transformation of Ag on a Cu-precovered Si( 111 ) surface. Surface Science, 2001, 493, 331-337.	1.9	4
213	Three-tiered Au nano-disk array for broadband interaction with light. Nanoscale, 2012, 4, 2847.	5.6	4
214	Nonlinear electron dynamics of gold ultrathin films induced by intense terahertz waves. Applied Physics Letters, 2014, 105, .	3.3	4
215	Sunlight absorbing titanium nitride nanoparticles. , 2015, , .		4
216	Optoelectronic characteristics of the Ag-doped Si p-n photodiodes prepared by a facile thermal diffusion process. AIP Advances, 2019, 9, 055024.	1.3	4

#	Article	IF	CITATIONS
217	Epitaxial growth mechanism of high-crystallinity lanthanum hexaboride (001) thin films on silicon (001) by electron beam deposition. Applied Physics Express, 2020, 13, 055504.	2.4	4
218	Photothermal heating and heat transfer analysis of anodic aluminum oxide with high optical absorptance. Nanophotonics, 2022, 11, 3375-3381.	6.0	4
219	Allotropic Transformation of Semimetal Bi Nanofilm on the Si Surface. Hyomen Kagaku, 2005, 26, 344-350.	0.0	3
220	Plasmon confinement in atomically thin and flat metallic films. , 2007, , .		3
221	Fabrication of Highly Dense Nanoholes by Self-Assembled Gallium Droplet on Silicon Surface. Materials Express, 2012, 2, 245-250.	0.5	3
222	Electron- and photon-induced plasmonic excitations in two-dimensional silver nanostructures. Applied Physics Letters, 2014, 104, 251117.	3.3	3
223	Sub-10 nm, high density titania nanoforests–gold nanoparticles composite for efficient sunlight-driven photocatalysis. Japanese Journal of Applied Physics, 2017, 56, 095001.	1.5	3
224	Role of Gap Size and Gap Density of the Plasmonic Random Gold Nanoisland Ensemble for Surface-Enhanced Raman Spectroscopy. Materials Transactions, 2018, 59, 1081-1086.	1.2	3
225	Optical Properties and Optimization of LaB <sub>6</sub> Thin Films for Photothermal Applications. Advanced Optical Materials, 0, , 2101787.	7.3	3
226	Tunneling conductivity features of the new reconstructed phases on the GaN(0001) surface. JETP Letters, 2003, 78, 578-582.	1.4	2
227	Ensemble of gold-patchy nanoparticles with multiple hot-spots for plasmon-enhanced vibrational spectroscopy. Proceedings of SPIE, 2016, , .	0.8	2
228	Harvesting Sunlight with Titanium Nitride Nanostructures. , 2018, , .		2
229	Transformation dynamics in Ca-induced reconstructions on Si(111) surface. E-Journal of Surface Science and Nanotechnology, 2003, 1, 26-32. Combined first-principles and electromagnetic simulation study of <mml:math< td=""><td>0.4</td><td>2</td></mml:math<>	0.4	2
230	xmlns:mml="http://www.w3.org/1998/Math/MathML"> <mml:mi>n</mml:mi> -type doped anatase <mml:math xmlns:mml="http://www.w3.org/1998/Math/MathML"&gt;<mml:mrow><mml:mi>Ti</mml:mi><mml:msub><mml:mi mathvariant="normal"&gt;O<mml:mn>2</mml:mn></mml:mi </mml:msub></mml:mrow> for</mml:math 	2.4	2
231	the applications in infrared surface plasmon photonics. Physical Review Materials, 2020, 4, . Structures and Electrical Conduction on Silicon Surfaces. Hyomen Kagaku, 1998, 19, 114-121.	0.0	1
232	Local electronic structure of a quantum point contact observed with STM. Physical Review B, 2006, 74, .	3.2	1
233	STM/STS STUDIES OF THE INITIAL STAGE OF GROWTH OF ULTRA-THIN BI FILMS ON 7 × 7-SI(111) SURFACE. International Journal of Nanoscience, 2007, 06, 399-401.	0.7	1
234	Enhanced photocatalytic activity of ultra-high aspect ratio ZnO nanowires due to Cu induced defects. Radiation Effects and Defects in Solids, 2015, 170, 939-944.	1.2	1

#	Article	IF	CITATIONS
235	Moiré nanosphere lithography: use colloidal moiré patterns as masks. Proceedings of SPIE, 2015, , .	0.8	1
236	Aluminum infrared plasmonic perfect absorbers for wavelength selective devices. Proceedings of SPIE, 2016, , .	0.8	1
237	UV-visible light photocurrent enhancement in STO thin films through metal-defect co-doping effect combined with Au plasmons. Materials Express, 2017, 7, 66-71.	0.5	1
238	Photocurrent Generation with Transition Metal Nitrides and Transition Metal Carbides. , 2018, , .		1
239	Metal/Conductive Oxide Plasmonic Structures for Surface-Enhanced Infrared Absorption Spectroscopy. Bunseki Kagaku, 2018, 67, 81-94.	0.2	1
240	Unconventional energy transfer from narrow to broad luminescent wide band gap materials. Europhysics Letters, 2019, 127, 17003.	2.0	1
241	Optical phase change in bismuth through structural distortions induced by laser irradiation. Radiation Effects and Defects in Solids, 2020, 175, 291-306.	1.2	1
242	Construction of an ELS–LEED: an electron energy-loss spectrometer with electrostatic two-dimensional angular scanning. , 2000, 30, 488.		1
243	Photocurrent generation from TiN nanostructures by visible light. , 2017, , .		1
244	Surfactant Growth and Optical Studies of Plasmonic Silver Nano-Disks. E-Journal of Surface Science and Nanotechnology, 2012, 10, 239-242.	0.4	1
245	STM/STS Studies of the Structural Phase Transition in the Growth of Ultra-Thin Bi Films on Si(111). Acta Physica Polonica A, 2003, 104, 381-387.	0.5	1
246	A temperature programmed desorption study of interactions between water and hydrophobes at cryogenic temperatures. Physical Chemistry Chemical Physics, 2022, 24, 16900-16907.	2.8	1
247	Bias dependence of STM profiles around the quantum point contact. Surface Science, 2006, 600, 4319-4322.	1.9	0
248	Growth of atomically flat nanofilms and surface superstructures of intrinsic liquid alloys. Applied Physics Letters, 2008, 92, 143116.	3.3	0
249	Relativistic Effect on the Bistability of Bi {012} Nanofilms. E-Journal of Surface Science and Nanotechnology, 2009, 7, 13-16.	0.4	0
250	Low-dimensional plasmons in atom-scale metallic objects. , 2010, , .		0
251	Topographically controlled growth of silver nanoparticle clusters. Physica Status Solidi - Rapid Research Letters, 2012, 6, 202-204.	2.4	0
252	Carrier Dynamics of a Bismuth Thin Film Accelerated via Intense Terahertz Field. , 2014, , .		0

ΤΑDΑΑΚΙ ΝΑGAO

#	Article	IF	CITATIONS
253	Nonlinear Carrier Responses in Gold Thin Films Induced by Intense Terahertz Waves. , 2014, , .		0
254	Nonlinear Carrier Dynamics in Semi-Metal Bismuth Induced by Intense Terahertz Field. , 2014, , .		0
255	Electron Dynamics in a Gold Thin Film Accelerated via an Intense Terahertz Field. , 2015, , .		0
256	Lossy plasmonic resonances in nanoparticles for broadband light absorption. , 2015, , .		0
257	Ultrafast carrier generation in Bi1-xSbx thin films induced by intense monocycle terahertz pulses. EPJ Web of Conferences, 2019, 205, 04016.	0.3	0
258	Editorial for the Special Issue "Infrared Nanophotonics: Materials, Devices and Applications― Micromachines, 2020, 11, 808.	2.9	0
259	Uniaxially oriented nickel aluminum superalloy films sputtered with in situ heating. Applied Physics Express, 2021, 14, 087001.	2.4	0
260	Plasmon-induced Charge Transport at Transition Metal Nitride-Semiconductor Interfaces via In Situ Nanoimaging. , 2021, , .		0
261	Fano resonance of optical phonons in a multilayer graphene stack. Japanese Journal of Applied Physics, O, , .	1.5	0
262	Observation of a two-dimensional plasmon in a metallic monolayer on silicon surface. Springer Proceedings in Physics, 2001, , 875-876.	0.2	0
263	Adsorption and Desorption of Au Nanoparticles Monitored by Infrared Spectroscopy. IEEJ Transactions on Electronics, Information and Systems, 2007, 127, 2171-2174.	0.2	0
264	Low-energy Plasmons in Ultrathin Silver Structures: a Combination of Electron Energy Loss and Infrared Spectroscopy. , 2011, , .		0
265	Surface Phonons of Lanthanum Hexaboride and its Thermionic Properties Shinku/Journal of the Vacuum Society of Japan, 1997, 40, 77-83.	0.2	0
266	Structures and Electrical Conduction on Silicon Surfaces Hyomen Kagaku, 1998, 19, 193-200.	0.0	0
267	Nonlinear Carrier Dynamics in Semi-metal Bismuth Induced by Intense Terahertz Field. Springer Proceedings in Physics, 2015, , 633-636.	0.2	0
268	Fabrication and Characterization of Moir $\tilde{A}$ $@$ Metasurfaces. , 2016, , .		0
269	Ultra-Narrowband Wavelength-Selective Thermal Emitter Designed by Bayesian Optimization. The Proceedings of the Thermal Engineering Conference, 2018, 2018, 0135.	0.0	0
270	Nonlinear terahertz dynamics of Dirac electrons in Bi thin films. , 2018, , .		0

#	Article	IF	CITATIONS
271	Enhanced photoelectrochemical water splitting by plasmonic Au nanostructures/reduced graphene oxide. , 2018, , .		Ο
272	Optical Excitation of Hot Carriers and Photothermal Conversions with Transition Metal Nitrides and Transition Metal Carbides. The Review of Laser Engineering, 2019, 47, 365.	0.0	0
273	Solar Water Distillation Using Titanium Nitride Nanostructures. Journal of the Society of Powder Technology, Japan, 2022, 59, 79-82.	0.1	0